

Grain reconstruction and determination of grain attributes from MD data sets of FCC polycrystals

P. W. Hoffrogge and L.A. Barrales-Mora[‡]

Institute of Physical Metallurgy and Metal Physics, RWTH Aachen University, 52056 Aachen, Germany

E-mail: barrales@imm.rwth-aachen.de

July 2016

Abstract. An algorithm for the identification and reconstruction of crystallites from molecular dynamics data sets of FCC materials was developed. The algorithm was tested in an Al polycrystal possessing a weak texture. For the conditions tested, the algorithm was able to find all of the input orientations and reconstruct the grains according to their crystallographic orientation. The method is capable of calculating specific attributes of grains, namely, volume, center of mass, average orientation and orientation spread. The method additionally provides a mapping method to track grains during time-row dataset. The software uses shared-memory parallelization implemented by the use of the OpenMP-API, which enables a fast analysis of large volumes of data with excellent performance.

Keywords: molecular-dynamics, grain reconstruction, post-processing, parallelization, grain growth, grain rotation

1. Introduction

In molecular dynamics (MD) simulations, the analysis and interpretation of the data remain a substantial and difficult part. Certain tools are required in order to reduce the amount of information and obtain useful quantities. In several situations, information on the evolution of 3D features is necessary, for example, grains in polycrystalline aggregates. This information is, however, not delivered by most of the available methods for the characterization of MD data sets. This task remains difficult because it involves identifying crystallographically the environment of the atoms to assign an orientation respective to a coordinate system and to reconstruct from this information the volume with identical orientation i.e., the grains. Due to the mathematical complexity of rotations and reconstruction algorithms, these calculations are slow and costly for their execution during runtime and even during post-processing if large data sets are involved. Nevertheless, several methods which enable the identification of crystal structures from

[‡] Corresponding author

atomic-based data have been already developed. The most straightforward way to distinguish between some of these is to compute the coordination number, i.e. the number of nearest neighbors (NNs) or next-nearest neighbors (NNNs) of the atoms. While this is a fast tool and also easy to implement, it obviously cannot distinguish between different atomic structures exhibiting the same coordination number. Another technique which allows a much more reliable identification of crystalline structures was first introduced by Honeycutt and Andersen [1]. This method analyzes the extent and connectivity properties of atom-diagrams which are comprised of nearest neighbors to two adjacent atoms. Based on this principle, also known as Common Neighbor Analysis or CNA, several algorithms have been implemented [2, 3, 4] and successfully performed to MD simulation data. Similarly, the centro-symmetry parameter, energy filters, bond order and angle and Voronoi analysis can also be used to discriminate atoms arranged in specific crystal structures [2]. Nevertheless, none of these methods can distinguish between groups of atoms with the same crystallographic orientation. To differentiate between differently oriented crystals, the definition of order parameters has been utilized. The drawbacks of this approach are that the orientations ought to be known beforehand and that complex rotations of the crystals might out-range the scope of the parameter. Nevertheless, this approach has been successfully utilized in numerous simulations to track, for instance, grain boundaries [5, 6, 7, 8, 9] and grain rotation [10, 11, 12, 13, 14].

The motivation of the present contribution is to introduce a method that allows the determination of the relative orientation of groups of atoms and reconstruct the grain from only this information. The method is able to generate a space-resolved three dimensional grain decomposition of atom-position data sets for FCC materials, such as generated by MD-simulations. The first step of the method calculates an orientation for each atom by taking into account the positions of the nearest-neighbor atoms. In a second step, the method generates grain entities from atoms with similar orientations by collecting them via nearest-neighbor paths. The method is capable of calculating grain specific properties, namely volume, center of mass, average orientation and orientation spread. The method additionally provides a mapping method in order to track grains during a time-row data set. The method is introduced in order to be able to track the grain growth evolution of individual grains during MD-simulations, additionally enabling a grain-resolved visualization of polycrystalline FCC data sets.

2. Methods

To identify the grains from a data set containing atomic positions, it is necessary to determine first the orientation of the atoms as a per-atom attribute from the local neighborhood. Once an atom (referred to as *central atom*) is selected arbitrarily, the calculation of the orientation proceeds in the following way:

- (i) Identify all the nearest neighbors and calculate the relative positions of the neighbors to the corresponding central atom.

- (ii) Determine the affine 3×3 transformation matrix M from the reference (non-rotated case) to the current crystal-configuration.
- (iii) Determine the rotation that best fits M as a least square solution.

All of these steps have an inherent mathematical and/or programmatic complexity. In the present section, we will discuss the algorithms that were utilized to solve each of these problems. In the appendix, these solutions are presented in the form of pseudo-code whereas the program is offered as an open-source project [15].

2.1. Orientation determination

The calculation begins with the identification of the nearest-neighbors. Once the neighbors of an atom have been identified, displacement vectors are calculated with the current atom as origin. These vectors are then normalized so that only unit vectors are used for the orientation calculation. Since in the FCC crystal structure each neighbor has an antipodal counterpart, the list of nearest neighbor vectors is reduced by finding vectors with a near 180° -relationship. The resulting mean direction \vec{v}_r is calculated by vector subtraction of any \vec{v} and its antipodal partner \vec{v}_a :

$$\vec{v}_r = \frac{1}{2}(\vec{v} - \vec{v}_a) \quad (1)$$

In the FCC lattice, there are three pairs of neighbor vectors, each lying on different $\{100\}$ planes. Since each vector ought to have only one defined perpendicular partner in the FCC-case, we try to find the directions of this planes by identifying vector pairs with a near 90° -relationship. Now, at least six different vectors must be available in order to find all three pairs. Afterwards, the $\langle 100 \rangle$ directions $v_{100}^{\vec{}}$ are calculated as the cross product of both pairs vectors \vec{v}_1 and \vec{v}_2 :

$$v_{100}^{\vec{}} = \vec{v}_1 \times \vec{v}_2 \quad (2)$$

The transformation matrix M can now easily be obtained as:

$$M = \begin{bmatrix} v_{x100} & v_{y100} & v_{z100} \\ v_{x010} & v_{y010} & v_{z010} \\ v_{x001} & v_{y001} & v_{z001} \end{bmatrix} \quad (3)$$

The assignment of the vectors to a certain row is of arbitrary nature, which can cause a negative determinant. It is possible to avoid this issue by calculating the determinant and checking whether it is negative or not. In the case that it results negative, the method inserts $-v_{100}^{\vec{}}$ in the first row instead of $v_{100}^{\vec{}}$. The matrix M is not necessarily a pure rotation matrix because the atoms can assume non perfect lattice positions due to elastic distortions or thermal vibrations. For this reason, we have to estimate the rotation that best fits the affine transformation defined by our matrix M . This problem is well known in aeronautics and thus, several solutions have been already provided in the

past. For instance, Horn [16] introduced a direct method that estimates an orientation from a set of corresponding vectors in two coordinate systems for aeronautical purposes. A similar method that requires computing the eigenvalues of a 4×4 matrix was presented by Bar-Itzhack [17]. This method is based on the q -method proposed by Keat [18]. We opted to use this method in the present contribution as operations with quaternions are computationally less expensive. The q -method utilizes a cost function c to be minimized:

$$c = \frac{1}{2} \sum_{i=1}^k a_i |\vec{b}_i - D(q)\vec{r}_i|^2 \quad (4)$$

where \vec{r}_i denotes a unit vector in the reference/sample coordinate system and \vec{b}_i the same vector in the body/crystal coordinate system. In turn, q is the sought rotation quaternion, which defines the rotation matrix D whereas a_i is an optional weight to each of the vector pairs. The cost function contains the square lengths of the error vectors, i.e. the minimization is applied with the Euclidean norm. In [18], it was shown that the solution of this problem is reduced to the computation of the eigenvalues of a symmetrical 4×4 matrix, which is defined by the set of vectors \vec{r}_i and \vec{b}_i . To find the best-fitting rotation quaternion to the transformation matrix, the method introduced in [17] was utilized. In Bar-Itzhack's contribution, it was shown that by utilizing the three base vectors [100], [010] and [001] of the reference coordinate system, the problem can be formulated for non-orthogonal matrices. As a result, the new matrix M_4 can be computed from the values of the matrix M from Eq. (3) as:

$$M_4 = \frac{1}{3} \begin{bmatrix} r_{11} - r_{22} - r_{33} & r_{21} + r_{12} & r_{31} + r_{13} & r_{23} - r_{32} \\ r_{21} + r_{12} & r_{22} - r_{11} - r_{33} & r_{32} + r_{23} & r_{31} - r_{13} \\ r_{31} + r_{13} & r_{32} + r_{23} & r_{33} - r_{11} - r_{22} & r_{12} - r_{21} \\ r_{23} - r_{32} & r_{31} - r_{13} & r_{12} - r_{21} & r_{11} + r_{22} + r_{33} \end{bmatrix} \quad (5)$$

The quaternion q representing the rotation that best fits M is the eigenvector of the most positive eigenvalue of M_4 . The quaternion q is assigned to the current atom during the calculation. In the case that the matrix M cannot be defined owing to strong lattice distortions, the corresponding atom is marked as non-oriented.

2.2. Grain detection

After the assignation of the orientation to the atoms, the grains are identified in a second step. The identification method uses the orientation information generated in the previous step. The procedure begins from an initial atom as a seed and recursive assignations are applied to nearest-neighbor atoms. For this, the following steps are conducted:

- (i) Check whether the nearest-neighbor atoms to a seed atom:
 - (a) are not yet assigned to another grain-entity.

- (b) own an orientation close to the seed-atom according to a user defined threshold (1° as default). This is referred to as the *local criterion*.
 - (c) own an orientation close ($< 3^\circ$ as default) to the mean orientation of the current grain if and only if enough atoms have been aggregated to this grain. This is referred to as the *global criterion*.
- (ii) If these conditions are fulfilled, the neighbor atom is aggregated. The procedure is now repeated from the beginning with the aggregated atoms as seeds.

This procedure is exercised for every atom in the data set. It can occur during an iteration that the number of aggregated atoms of a grain is smaller than a reasonable amount (200 atoms as default). Whenever this happens, the corresponding grain information is removed and all collected atoms during this step are set to be unassigned again.

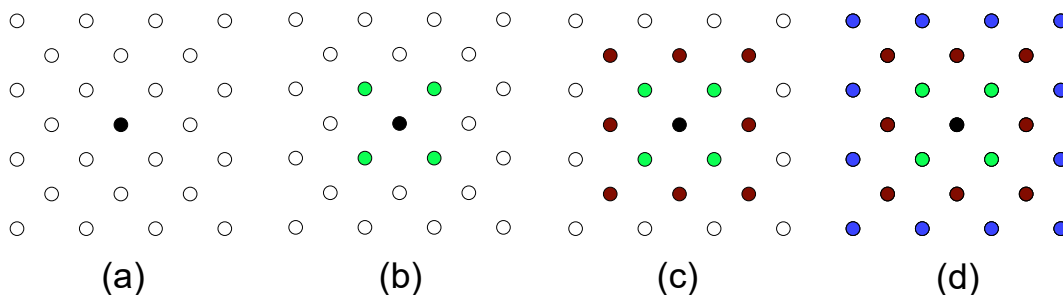


Figure 1: Sequence for the identification of the grains. (a) A seed atom is selected from the dataset; open circles represent atoms with the same orientation as the seed atom. (b) The first neighbors to the seed are identified by comparison of the per-atom orientations and collected into a grain entity. (c-d) In subsequent iterations, the already identified atoms (green in (c), brown in (d)) act as seeds for their next-neighbors. Atoms are continually collected until no equally oriented atoms can be found in an iteration step.

In Fig. 2, the application of the misorientation criteria is exemplified. The *local criterion* compares the orientation of two atoms in a nearest-neighbor relationship whereas the *global criterion* assures that the orientation of an atom to be aggregated has a similar orientation than that of the current grain. The *global criterion* allows for the detection of grains separated by low angle grain boundaries, which otherwise cannot be detected only by local comparisons due to the gradual change of orientation between grains at positions far away from dislocation centers.

2.3. Orphan atom adoption

In some cases owing to strong thermal vibrations or proximity to lattice defects, the determination of the orientation can fail or deliver orientations different than those found in an immediate neighborhood. In both cases, such atoms will not be assigned to a grain entity during the grain identification step. These atoms, deemed in the following

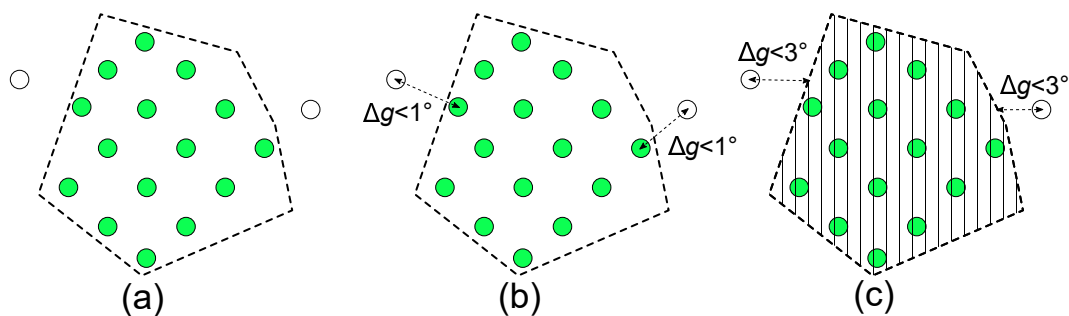


Figure 2: A fully identified grain (a) consists of the atoms (solid circles) enclosed by the dashed line after few iterations. Nearest-neighbors to the already aggregated atoms are tested in subsequent iterations. In order to collect an atom to the current grain entity, the atom must have an orientation difference less than 1° with respect to the seed atom (b) and additionally ensure that the orientation difference with respect to the mean orientation of the grain is less than 3° (c).

as *orphan atoms*, can cause a substantial underestimation of the volume of the grains. To solve this problem, we utilized a method inspired in noise correction methods used in EBSD mapping algorithms [19, 20]. The approach consists of the following steps:

- (a) For each orphan atom, the grains to which the nearest neighbors belong are identified and counted.
- (b) From the list of grains determined in the previous step, the one with most occurrences is selected.
- (c) If the maximum number of occurrences is higher than a user defined value (the default is three), the orphan atom is assigned to the grain selected in step (b).
- (d) The procedure is repeated for all remaining orphan atoms.

The minimum number of grain occurrences (three) was introduced in order to suppress random grain assignments. This procedure is schematically shown in Fig. 3. Note that initially (Fig. 3b) only orphan atoms a_A and a_B are adopted because only they had enough nearest neighbors assigned to a common grain. This procedure is applied iteratively so that the number of orphan atoms is reduced to a minimum.

2.4. Grain-tracking over time

In order to determine the evolution of grain properties over time, it is necessary to track the grains from snapshots generated at different times. To do this, we assume that geometrical and orientation attributes of the grains show little change between subsequent time states. This enables finding correspondence of grains by comparing calculated properties. We utilized two criteria to identify possible corresponding candidates, namely the center-of-mass (COM) and the misorientation between grain candidates. To begin with, the COM of the grains is calculated for the data sets generated at times t and $t + \Delta t$. An arbitrary grain G_1 is selected from the second

data set ($t + \Delta t$). From the first one (t), the grains that fulfill $d \leq d_{max}$, where d is the distance to grain G_1 and d_{max} is a user defined threshold value, are chosen. This list is further refined by rejecting grains with a misorientation larger than a user-defined value ($\Delta g > 5^\circ$ as default). If more than one grain exist that fulfill both criteria, the grain with the shortest distance d is chosen.

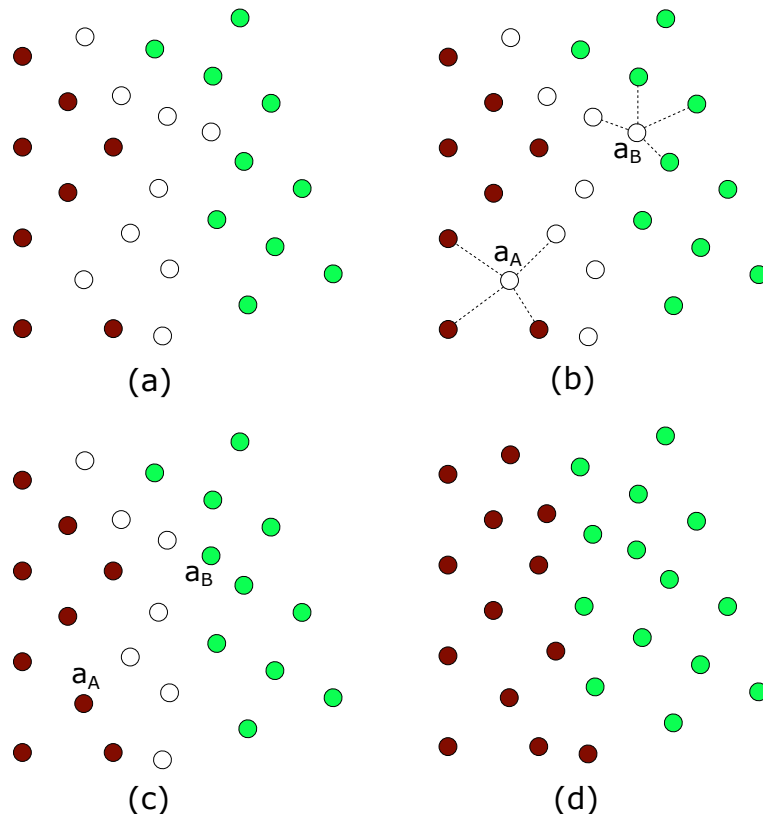


Figure 3: Adoption of orphan atoms. The orphaned state is represented by open circles whereas differently colored circles signify atoms aggregated to different grains. (a) Initially, many atoms close to grain boundaries are not assigned to a specific grain. These atoms are adopted recursively depending on the frequency occurrences to neighboring grains (b). For example, in (c) atom a_A is adopted by the grain on the left whereas atom a_B is adopted by the grain on the right. After a few iterations the number of orphan atoms is reduced to a minimum (d).

The methods described in the previous sections are provided as pseudo-code in the appendix and implemented as a command-line program called GraDe-A (Grain Detection Algorithm). The program was written in the object-oriented C++ programming language. Furthermore, the software uses shared-memory parallelization by means of the OpenMP-API [21], which enables analyzing several input files in parallel. The code has been written accounting for computation time considerations. Thereby, the utilization of computationally slow operations such as square root or cosine calculations has been avoided. Additionally, the computation domain has been split into cells in order to accelerate nearest-neighbor-search algorithms. All orientation data is

internally stored as unit quaternions with memory consumption for only four floating-point numbers. Therefore, all misorientation calculations are implemented as simple quaternion operations, which are superior to rotation matrix operations with regard to computational effort. Unique cubic orientation quaternions [22] are used in order to be able to calculate the mean-orientation and the orientation spread [22] for each grain. Additionally, this enables to use a fast disorientation calculation for the grain identification algorithm. The code is also offered as open-source software [15].

2.5. Molecular dynamics simulations of grain growth

Molecular dynamics simulations were employed to test the developed software. For this purpose, nanocrystalline grain growth was simulated. The large-scale atomic/molecular massively parallel simulator (LAMMPS) code [23] was utilized. The atomic interactions were described by the EAM potential for Al developed by Mishin et al. [11]. The algorithms presented in previous sections were used to determine the orientation of grains in an Al polycrystal and reconstruct them in time-resolved molecular dynamics data sets [15]. The simulation block used in these MD simulations was composed of one hundred Voronoi grains with different orientations (Fig. 4) that were defined so that a weak texture was predominant in the microstructure. The orientations were assigned randomly to the grains. The simulation box had a side length of 43.27 nm in all directions and contained 4834137 atoms for an initial average grain size of approximately 11.57 nm. Periodic boundary conditions were used on all the surfaces of the simulation box. Before the MD simulation was performed, the energy of the system was minimized by the conjugate-gradient algorithm. Subsequently, damped dynamics were applied to fully relax the grain boundaries. The isothermal-isobaric (NPT) ensemble was used for the time integration with a time step of 0.2 fs. The simulation was performed at 500 °C. The total simulation time corresponded to 4 ns. In order to warrant the accuracy of the measured properties of the simulated systems, snapshots were regularly saved in intervals of 0.01 ns. The obtained configurations were subsequently quenched computationally in an NPT-ensemble for a time of 0.1 ns to a target temperature of 1 K and additionally relaxed by the conjugate gradient algorithm after setting the kinetic energy to zero. For the identification of the grains, the default thresholds were consistently used for all of the data analyzed. An amount of 200 atoms was set as a minimum for any grain detection.

The MD-simulations were performed on the Jülich Supercomputing Cluster and the post-processing of the data on the RWTH-Aachen Computer Cluster.

3. Results

The algorithm was benchmarked on a Bull MPI-S machine possessing Intel Xeon X5675 processors. For these tests, we used 24 files of approximately 240 MB containing ~ 4.8 million atoms. The utilized parallelization scheme allowed reducing the computation

time from 1.02 hours for two threads to only 12 minutes for 12 threads (Table 1). Irregular scaling with the number of threads was observed. This behavior was caused by an asymmetrical distribution of tasks per thread seen in situations where the number of tasks is not a multiple of the number of threads e.g. 10 threads. This problem is less significant with an increasing number of tasks. For instance, in the present contribution a total of 400 files for a total data volume of 140 GB were evaluated in only approximately 4 hours.

Table 1: Comparison of the total computation time t_{comp} necessary for processing 24 output-files by the Grade-A tool. A different number of threads (#Th) were used for benchmarking in a linux-environment with 12 CPU-cores. Each file contained about 4.8 million atoms and had a size of approximately 240 MB. The relative overhead was calculated using the computation with two threads as reference.

#Th	$t_{comp}(h)$	$t_{comp} \times \#Th$ (h)	Overhead (%)
2	1.02	2.03	0.00
4	0.53	2.12	3.78
6	0.37	2.23	9.469
8	0.29	2.28	12.17
10	0.28	2.77	36.10
12	0.20	2.43	19.29

To estimate the accuracy of the algorithm, the determined orientations were compared to the ones used as input. It is stressed that the algorithm does not require initial orientations as input. The figures plotted in Fig. 4 illustrate clearly that the algorithm is capable to identify correctly the orientations of the grains. Fig. 4a and Fig. 4b correspond respectively to the seeded orientations and the orientations calculated from the MD data set. Fig. 4c shows the microstructure colored after the identification number of the grains, which is a number determined by the sorted volume of the grains. This is the reason, why large grains appear blue and small red. The identification number can change from one snapshot/time-step to another due simply to the growth and shrinkage of the grains. However, as explained in the previous section the algorithm is capable of tracking correctly the grains as the COM and orientation are the criteria utilized for the tracking, independently of the identification number assigned at a time step.

Clearly, the advantage of the grain reconstruction is that it makes possible the tracking of grain properties such as volume, center of mass, average orientation, orientation spread and orientation change. Additionally, the algorithm permits the identification of sudden events that influence decisively the development of the microstructure. For instance, Fig. 5a illustrates the global kinetics obtained by detecting the remaining grains at each snapshot of the simulation. It is noted that since grains are individually identified, other algorithms for grain size measurements, such as fitting ellipsoids to the grains [24], can be easily implemented.

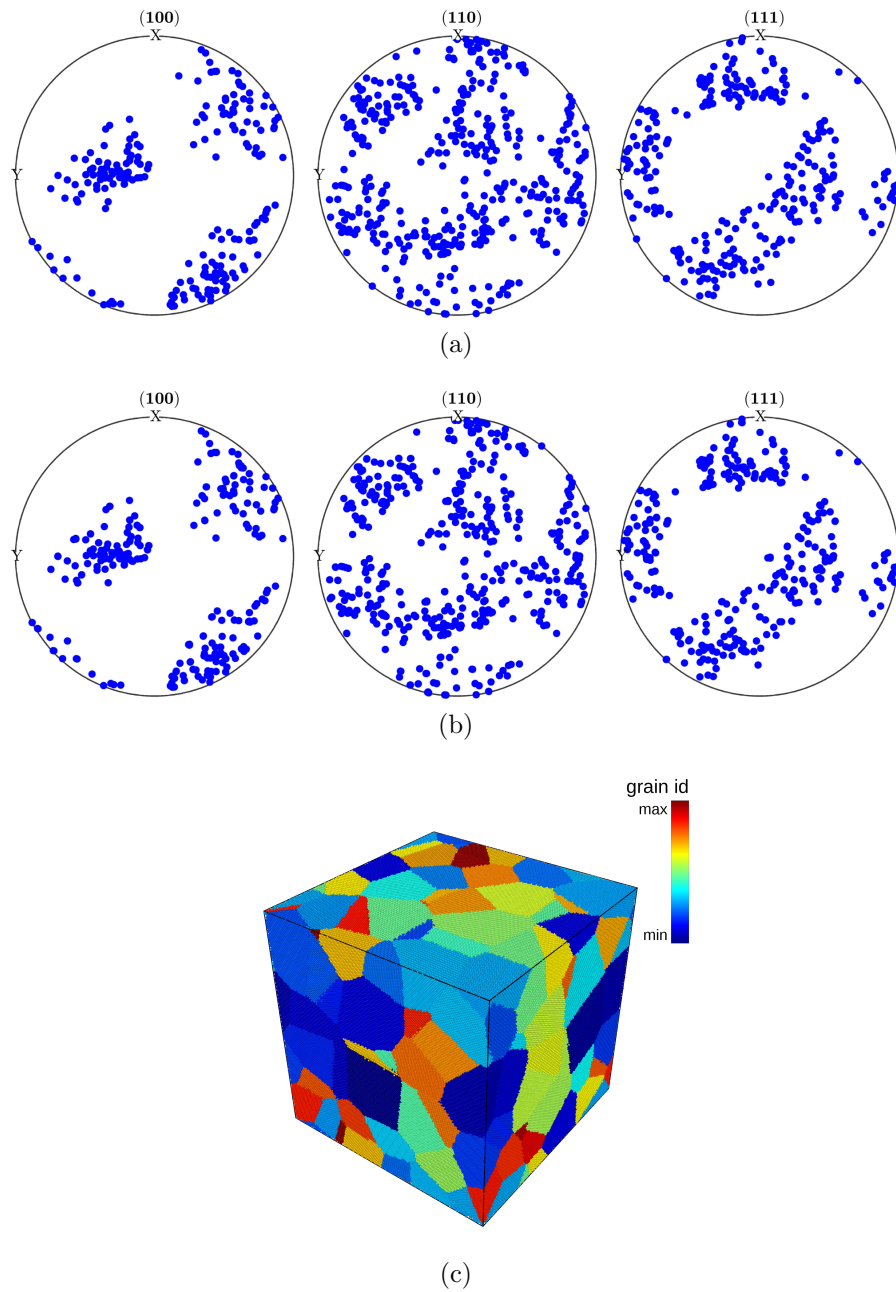


Figure 4: (a) The input orientation are shown in the pole figures and (b) compared to the determined orientations by the GraDe-A tool. An excellent agreement can be observed. The reconstruction of the grains is seen in (c), where the grains are colored according to an integer number that serves as an id for the grains. This number was assigned so that the smallest number corresponds to grains with the largest volume and vice versa.

In turn, Fig. 5b shows the individual kinetics of the detected grains. Note that the ordinate is in logarithm scale so that the collapse of the grains is better visualized. For comparison, the orientations of the remaining grains after the finalization of the

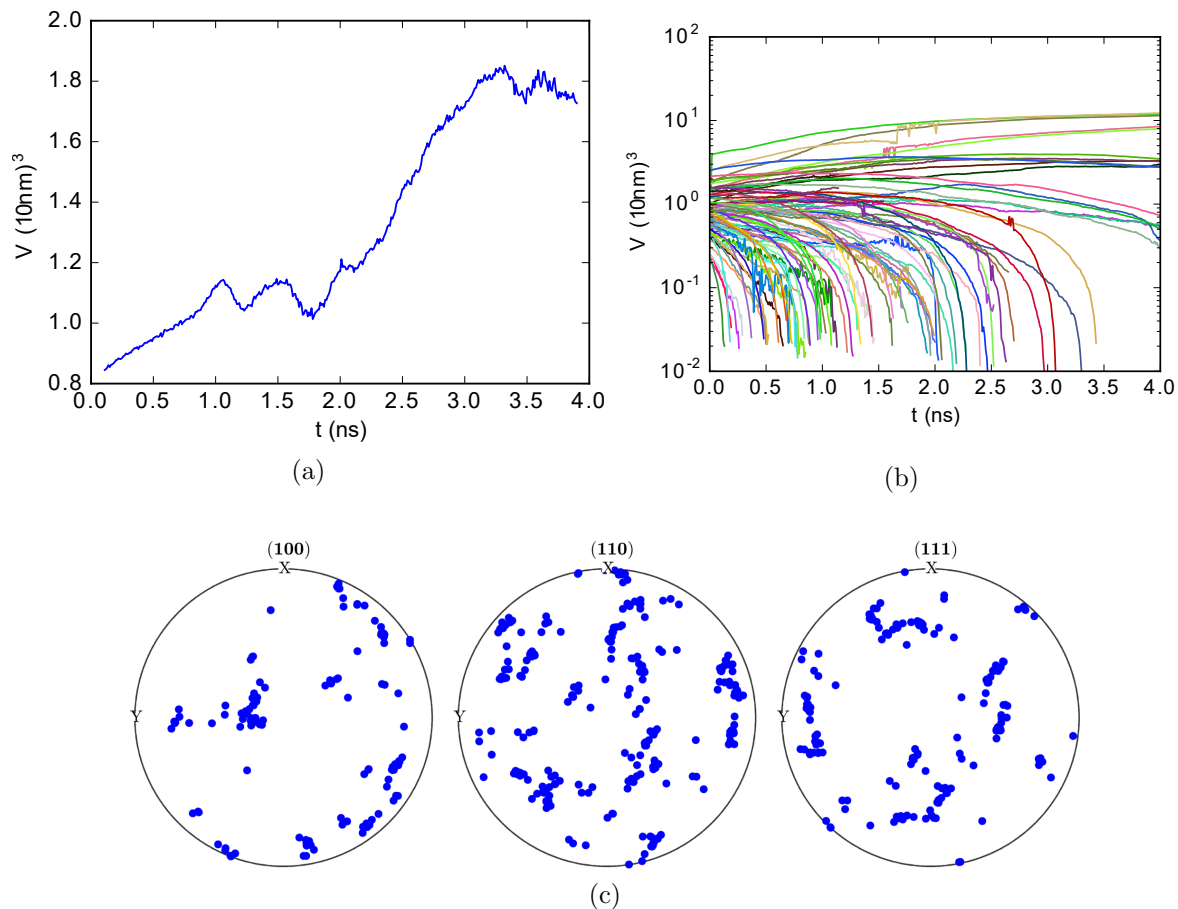


Figure 5: (a) Global kinetics, (b) individual kinetics and final texture (c) after 4 ns of computational annealing at 500 °C.

simulation are plotted in the pole figures shown in Fig. 5c; a slight sharpening of the initially used weak texture is evident as expected for the texture evolution after grain growth [25]. Since the algorithm is capable to determine a per-atom orientation and identify the grains, it is also possible to determine any change in orientation that might be induced during grain growth. This is a topic of interest because Cahn and Taylor [26] predicted that rotation of grains can be caused by the motion of grain boundaries. Several simulation studies [12, 13, 27, 14, 28] and some experimental ones [29, 30] have confirmed this effect for stressed nanocrystalline polycrystals. However, other experimental studies [31] have not observed this concomitant grain migration and rotation in systems closer to the simulated ones, where rotation is thought to be more prominent. In fact, in previous simulation studies [14, 32], we showed that rotation is strongly dependent on the character of the grain boundary. Furthermore, most of the computational studies have been performed in bi- or tricrystals [27] and with CSL grain boundaries as a necessity to fulfill periodicity on all surfaces of the simulation setups. However, grain boundaries in real microstructures tend to be of a mixed and general character and deviate substantially from CSL or Σ grain boundaries. For this

reason it is unclear whether rotation will be observed as a generalized mechanism of microstructure evolution. To investigate if grain rotation is observed in nanocrystalline polycrystals subjected to grain growth, we tracked the orientation change of the grains. In Fig. 6a the average absolute change of grain orientation as a function of time is shown. The maximum orientation change was less than 3.5° ; this evinced only a marginal orientation change that is not in accordance with Cahn and Taylor theoretical expectations [26, 14, 32, 13]. The reason for this may be related to the structure of the grain boundaries as discussed in [14] but a more detailed investigation of the mechanisms of grain boundary migration is necessary to affirm this. As for the kinetics, the change of orientation can also be resolved for individual grains. This is illustrated in Fig. 6b, where the rotation of all the grains in the simulations is plotted as a function of time. Interestingly, rotation is most prominent for grains that are close to collapse as evinced by those grains, whose orientation change increases in a very short time.

To give an impression of the practicality of the algorithm, individual grain kinetics and orientation change for an arbitrary grain are shown in Fig. 6c and Fig. 6d. This representation makes possible identifying significant but rare events that are determinant for microstructure evolution [33, 34, 35, 36]. In the case of this grain, the kinetics showed an initial fast growth until it reached a constant volume from approximately 2 to 2.5 ns. Afterwards, the grain shrank until the simulation finished. The morphology of this grain can be seen in Fig. 7. This grain was able to survive the whole simulation and grew successfully for most of its life reaching a maximum grain size after 2.66 ns (Fig. 7c). This growth is also substantiated by the number of faces that the grain gained. For instance, after 1.33 ns (Fig. 7b) the grain had significantly more faces than originally (Fig. 7a) and evidently a concave shape that signifies positive growth rates. At the last simulated time (Fig. 7d), the grain had already started shrinking showing a smaller size than at a previous time (Fig. 7c) and also a convex shape. Note that the shape is not irregular and approximates excellently grains observed in polycrystals by serial-sectioning or tomography [37, 38, 39]. This is also an indication that the software can identify and reconstruct the grains adequately. In the same manner, the evolution of single grains showing interesting features can be followed visually by discriminating them from the data set of identified grains. For instance, this tool was already utilized to investigate size-effects observed in nanocrystalline materials; this will be the issue of a future contribution.

The purpose of this manuscript was to introduce the computational tool GraDe-A for the determination, reconstruction and tracking of grains in FCC polycrystals from MD data sets. This tool can be utilized to evaluate the change of properties of the grains and we expect it to become a valuable tool for the interpretation of data from MD simulations. Recently, also a tool capable of discerning orientation from MD datasets was developed [40], which in conjunction with the tool here introduced would allow analyzing grains in polycrystals with different crystal structures.

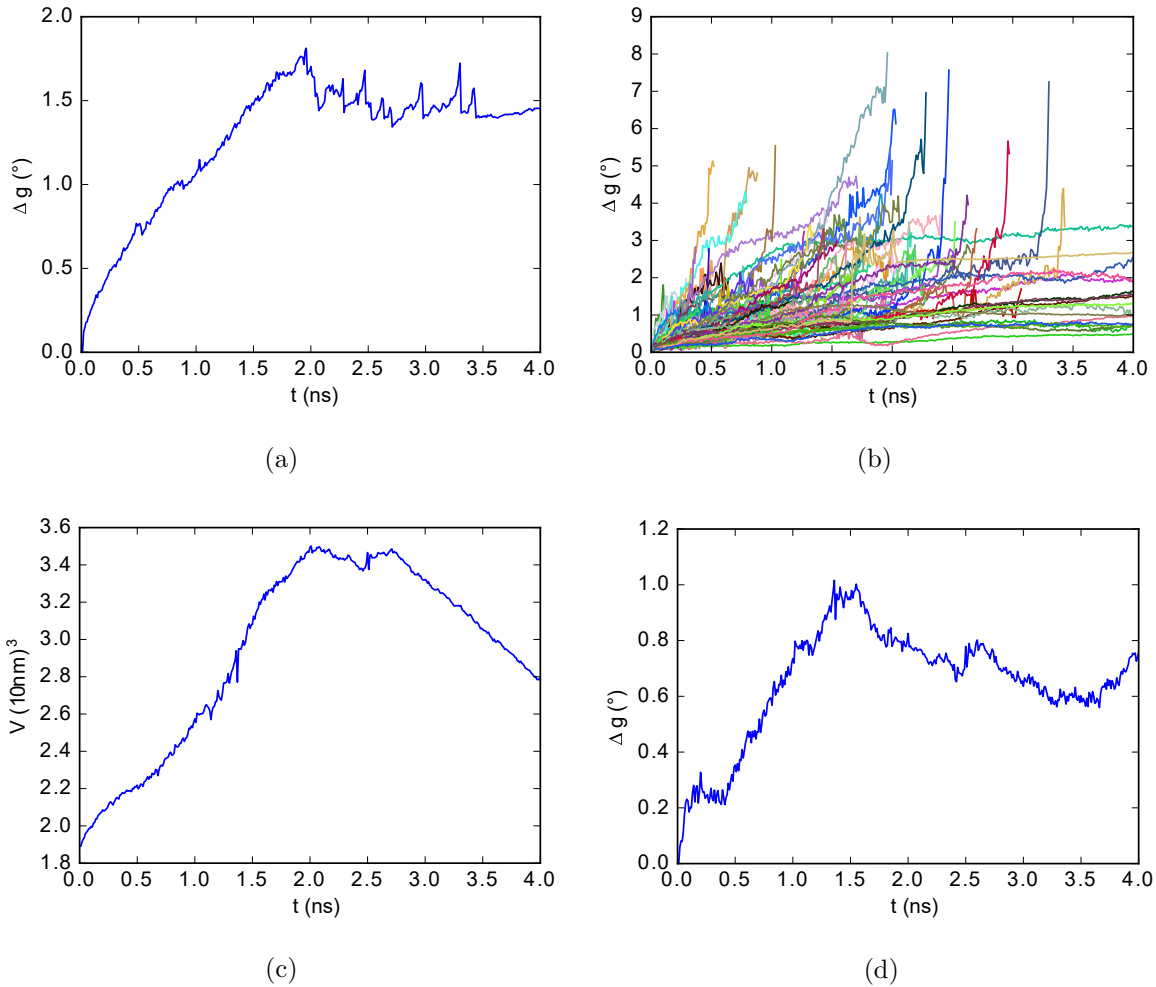


Figure 6: (a) Average grain rotation and (b) individual rotation of the grains. Grain rotation seems to increase with decreasing grain size of the grains. However, the average orientation change of the grains remains below 3.5° . Significant events for microstructure evolution can also be identified since properties such as kinetics (c) and orientation change (d) of the grains are individually resolved. In (c) and (d), the properties plotted correspond to the grain shown Fig. 7

4. Summary

A computational tool, which is capable of identifying grain entities by the calculation of per-atom orientation quaternions, was developed. It was demonstrated that the tool is powerful enough to allow for grain-resolved 3D-visualizations of the grains and that it provides useful grain-quantities, such as mean-orientation, volume and rotation angles. A Voronoi-tesselated microstructure with a weak texture was synthesized and used to simulate grain growth at 500°C by molecular dynamics; snapshots from these simulations were used to benchmark the computational tool. The developed algorithm was used to determine global and per-grain kinetics and mean rotation of the grains.

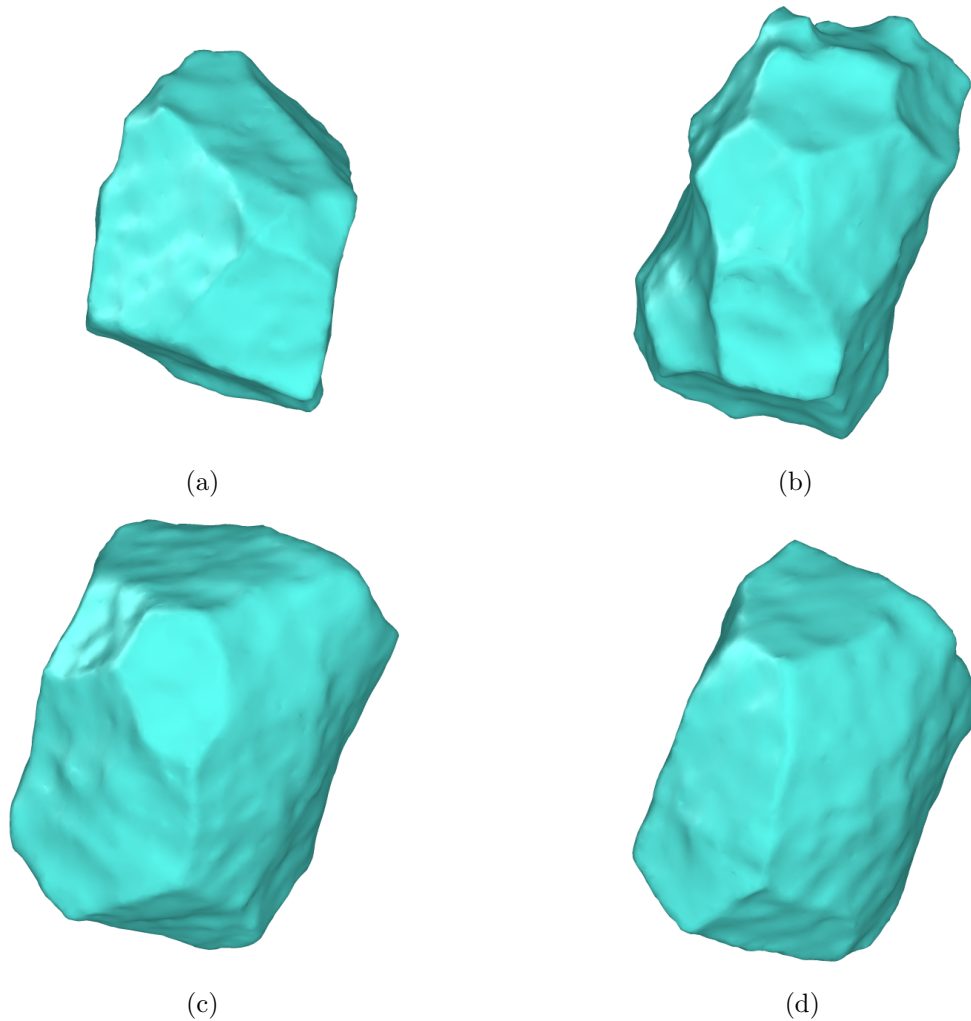


Figure 7: Development of an arbitrary grain as reconstructed by the GraDe-A tool. The surface was calculated by means of the visualization software OVITO [41]. This grain initially grew (b) until it reached a maximum number of faces after 1.33 ns and a maximum size (c) after 2.66 ns. Afterward, the grain shrank (d) until the simulation finalized after 4 ns.

Additionally to these capabilities, there are various improvements and extensions that are currently under development:

- Add support for other lattice-structures
- Identifying and highlighting other network-entities such as faces, edges and junctions
- Calculate grain-properties such as triple line length, turning angle and mean width
- Obtaining topological and connectivity-information for each grain
- Calculating the 5 parameter space of grain boundaries
- Determination of Bernal structures of grain boundaries

- Automatically identify grain-coalescence events

These enhancements would be helpful for the analysis of nanocrystalline grain growth and rotation since most of the processes observed are difficult to discuss without knowing exact information on the involved defects and geometries.

Acknowledgements

The authors express their gratitude to the Deutsche Forschungsgemeinschaft (DFG) for financial support (Grants GO 335/44-1) and gratefully acknowledge the computing time granted (JHPC24) by the John von Neumann Institute for Computing (NIC) and provided on the supercomputer JURECA at Jülich Supercomputing Centre (JSC). P. W. Hoffrogge thankfully acknowledges the computing time granted by the RWTH-Aachen University (RWTH0060) for the execution of his master-thesis project.

References

- [1] Honeycutt J D and Andersen H C 1987 *The Journal of Physical Chemistry* **91** 4950–4963 ISSN 0022-3654 1541-5740
- [2] Stukowski A 2012 *Modelling and Simulation in Materials Science and Engineering* **20** 045021 ISSN 0965-0393 1361-651X
- [3] Stukowski A and Albe K 2010 *Modelling and Simulation in Materials Science and Engineering* **18** 085001 ISSN 0965-0393 1361-651X
- [4] Begau C, Hua J and Hartmaier A 2012 *Journal of the Mechanics and Physics of Solids* **60** 711–722 ISSN 00225096
- [5] Janssens K G F, Olmsted D, Holm E A, Foiles S M, Plimpton S J and Derlet P M 2006 *Nature Materials* **5** 124–127 ISSN 1476-1122 1476-4660
- [6] Zhang H, Mendeleev M and Srolovitz D 2005 *Scripta Materialia* **52** 1193–1198 ISSN 13596462
- [7] Zhang H, Mendeleev M I and Srolovitz D J 2004 *Acta Materialia* **52** 2569–2576 ISSN 13596454
- [8] Zhang H, Srolovitz D J, Douglas J F and Warren J A 2007 *Acta Materialia* **55** 4527–4533 ISSN 13596454
- [9] Zhang H, Upmanyu M and Srolovitz D J 2005 *Acta Materialia* **53** 79–86 ISSN 13596454
- [10] Mishin Y, Asta M and Li J 2010 *Acta Materialia* **58** 1117–1151 ISSN 13596454
- [11] Mishin Y, Farkas D, Mehl M J and Papaconstantopoulos D A 1999 *Physical Review B* **59** 3393–3407 ISSN 0163-1829 1095-3795
- [12] Trautt Z T, Adland A, Karma A and Mishin Y 2012 *Acta Materialia* **60** 6528–6546 ISSN 13596454
- [13] Trautt Z T and Mishin Y 2012 *Acta Materialia* **60** 2407–2424 ISSN 13596454
- [14] Barrales-Mora L A, Brandenburg J E and Molodov D A 2014 *Acta Materialia* **80** 141–148 ISSN 13596454
- [15] Hoffrogge P W and Barrales-Mora L A 2016 <https://github.com/paulhof/GraDe-A> URL <https://github.com/paulhof/GraDe-A>
- [16] Horn B K P 1987 *Journal of the Optical Society of America a-Optics Image Science and Vision* **4** 629–642 ISSN 0740-3232 g6126 Times Cited:1602 Cited References Count:15 URL <GotoISI>://WOS:A1987G612600002
- [17] Bar-Itzhack I Y 2000 *Journal of Guidance, Control, and Dynamics* **23** 1085–1087 ISSN 0731-5090 1533-3884
- [18] Keat J 1977 Analysis of least-squares attitude determination routine doaoop Report Technical Report CSC/TM-77/6034, Comp. Sc. Corp
- [19] Humphreys F J 2001 *Journal of Materials Science* **36** 3833–3854 ISSN 00222461

- [20] Humphreys F J 2004 *Scripta Materialia* **51** 771–776 ISSN 13596462
- [21] Dagum L and Menon R 1998 *Computational Science & Engineering, IEEE* **5** 46–55
- [22] Cho J H, Rollett A D and Oh K H 2005 *Metallurgical and Materials Transactions A* **36** 3427–3438 ISSN 1543-1940 URL <http://dx.doi.org/10.1007/s11661-005-0016-4>
- [23] Plimpton S 1995 *Journal of Computational Physics* **117** 1–19 ISSN 00219991
- [24] Groeber M A and Jackson M A 2014 *Integrating Materials and Manufacturing Innovation* **3** 5 ISSN 2193-9772
- [25] Barrales-Mora L 2008 *2D and 3D Grain Growth Modeling and Simulation* (Göttingen: Cuvillier) ISBN 9783736926844 URL <http://books.google.de/books?id=E3Q0YNZod0wC>
- [26] Cahn J W and Taylor J E 2004 *Acta Materialia* **52** 4887–4898 ISSN 13596454
- [27] Trautt Z T and Mishin Y 2014 *Acta Materialia* **65** 19–31 ISSN 13596454
- [28] Upmanyu M, Srolovitz D J, Lobkovsky A E, Warren J A and Carter W C 2006 *Acta Materialia* **54** 1707–1719 ISSN 13596454
- [29] Harris K E, Singh V V and King A H 1998 *Acta Materialia* **46** 2623–2633 ISSN 13596454
- [30] Legros M, Gianola D S and Hemker K J 2008 *Acta Materialia* **56** 3380–3393 ISSN 13596454
- [31] Mompioni F, Legros M, Radetic T, Dahmen U, Gianola D S and Hemker K J 2012 *Acta Materialia* **60** 2209–2218 ISSN 13596454
- [32] Brandenburg J E, Barrales-Mora L A and Molodov D A 2014 *Acta Materialia* **77** 294–309 ISSN 13596454
- [33] Haslam A J, Moldovan D, Phillpot S R, Wolf D and Gleiter H 2002 *Computational Materials Science* **23** 15–32 ISSN 0927-0256 556VW Times Cited:35 Cited References Count:74 URL <http://www.isinet.com/000175870500003>
- [34] Haslam A J, Moldovan D, Yamakov V, Wolf D, Phillpot S R and Gleiter H 2003 *Acta Materialia* **51** 2097–2112 ISSN 1359-6454 665TW Times Cited:75 Cited References Count:31 URL <http://www.isinet.com/000182138200023>
- [35] Haslam A J, Phillpot S R, Wolf H, Moldovan D and Gleiter H 2001 *Materials Science and Engineering a-Structural Materials Properties Microstructure and Processing* **318** 293–312 ISSN 0921-5093 510EX Times Cited:89 Cited References Count:73 URL <http://www.isinet.com/000173196700034>
- [36] Haslam A J, Yamakov V, Moldovan D, Wolf D, Phillpot S R and Gleiter H 2004 *Acta Materialia* **52** 1971–1987 ISSN 1359-6454 814VD Times Cited:24 Cited References Count:56 URL <http://www.isinet.com/000221001300020>
- [37] Rhines F N 1986 *Dr. Riederer Verlag GmbH, 1986* 93
- [38] McKenna I M, Poulsen S O, Lauridsen E M, Ludwig W and Voorhees P W 2014 *Acta Materialia* **78** 125–134 ISSN 13596454
- [39] Mbus G and Inkson B J 2007 *Materials Today* **10** 18–25 ISSN 13697021
- [40] Peter Mahler L, Sren S and Jakob S 2016 *Modelling and Simulation in Materials Science and Engineering* **24** 055007 ISSN 0965-0393 URL <http://stacks.iop.org/0965-0393/24/i=5/a=055007>
- [41] Stukowski A 2010 *Modelling and Simulation in Materials Science and Engineering* **18** 015012 URL <http://stacks.iop.org/0965-0393/18/i=1/a=015012>

Appendix A. Appendix

Appendix A.1. Per-atom orientation calculation

An orientation is calculated by algorithm A1 for every atom by taking into account the positions of the nearest neighbors. During the calculation a reduced neighbor vector list V_R is calculated for every atom by algorithm A2. This procedure eliminates double occurrences of anti-parallel neighbor unit-vectors by calculating the mean direction

$1/2(v_i - v_j)$ of near antipodal pairs. If a sufficient amount of directions remains, the orientation calculator utilizes them to formulate a transformation matrix M , as described in section 2.1. In order to obtain the largest eigenvalue as the resulting quaternion q we use the external open-source linear-algebra solver Armadillo[§].

[§] <http://arma.sourceforge.net>

Algorithm A1: Algorithm calculating the orientation of an atom in a fcc-lattice structured material by taking into account the near neighborhood.

Input: The antipodal threshold angle $\Delta\alpha$ and the perpendicular threshold angle $\Delta\beta$ in the current work chosen to be 5° and 11.5° , respectively.

```

1 foreach atom  $a$  do
2   Identify all  $n_{NN}$  nearest neighbor atoms  $A_{NN}$ 
3   Calculate the relative positions  $V_{NN}$  of  $A_{NN}$  to  $a$ 
   // The fcc-lattice has twelve neighbors, too much neighbors may cause
   // problems.
4   if  $n_{NN} > 12$  then
5     | return not oriented
6   end
7   Calculate the unit vectors to  $V_{NN}$  and save them in  $V_{NN}$ 
   // Find the antipodal partners and calculate the mean direction
8   Use algorithm A2 to generate the reduced vector list  $V_R$  containing  $n_R$  vectors
   // For the fcc-lattice at least 6 neighbor directions need to be available
9   if  $n_R < 6$  then
10    | return not oriented
11  end
   // Calculate three  $\langle 100 \rangle$  directions
12  Empty  $\langle 100 \rangle$ -vector list  $V_{100}$ 
13  for  $i = 0; i < n_R; i++$  do
14    |  $\vec{v}_i$  is the  $i$ th vector in  $V_R$ 
15    | if the number of vectors inside  $V_{100}$  is three then
16    |   | break
17    | end
   // check all  $ij = ji$  combinations
18    | for  $j = i + 1; j < n_R; j++$  do
19    |   |  $\vec{v}_j$  is the  $j$ th vector in  $V_R$ 
20    |   | if the angle between  $\vec{v}_i$  and  $\vec{v}_j$  is in the interval  $90^\circ \pm \Delta\beta$  then
21    |   |   | // Calculate the crossproduct of  $\vec{v}_i$  with  $\vec{v}_j$ 
22    |   |   |  $v_{\vec{CP}} = \vec{v}_i \times \vec{v}_j$ 
23    |   |   | Append  $v_{\vec{CP}}$  to  $V_{100}$ 
24    |   |   | if the number of vectors inside  $V_{100}$  is three then
25    |   |   |   | break
26    |   |   | end
27    |   | end
28    | end
29  | if the number of vectors inside  $V_{100}$  is smaller than three then
30  |   | return not oriented
31  | end
32  Setup the matrix  $M$  as shown in equation (3)
33  Calculate the orientation quaternion  $q$  as a least square solution to  $M$ , utilizing a
    $4 \times 4$ -Matrix and computing the corresponding eigenvectors with Armadillo
34  return the orientation id to  $q$ 
35 end

```

Result: The orientation id to the atoms orientation

Algorithm A2: Algorithm reducing a nearest neighbor vector list by eliminating twice occurrences of antipodal vectors.

Input:

Vector list V_{NN} containing n_{NN} nearest neighbor unit-vectors of an atom

The antipodal threshold angle $\Delta\alpha$

```

1 Empty reduced-vector list  $V_R$ 
2 for  $i = 0; i < n_{NN}; i++$  do
3    $v_i$  is the  $i$ th vector in  $V_{NN}$ 
   // check all  $ij = ji$  combinations
4   for  $j = i + 1; j < n_{NN}; j++$  do
5      $v_j$  is the  $j$ th vector in  $V_{NN}$ 
6     if both  $v_i$  and  $v_j$  are unpaired then
7       if the angle between  $v_i$  and  $v_j$  is in the interval  $180^\circ \pm \Delta\alpha$  then
8         Append  $\frac{1}{2}(v_i - v_j)$  to  $V_R$ 
9          $v_i$  and  $v_j$  are marked as paired
10        end
11      end
12    end
    // Poor  $v_i$  didn't find a partner ?
13    if  $v_i$  is still unpaired then
14      Append  $v_i$  to  $V_R$ 
15    end
16 end

```

Result: The reduced vector list V_R

Appendix A.2. Grain identification and reconstruction

In order to group atoms together into a grain entity, two different criteria were introduced. A *local criterion* that compares the orientation of a candidate atom i.e. that of the atom to be assigned to a certain grain and that of the reference atom, referred to as parent atom. A *global criterion* compares the average orientation of the grain and the orientation of the candidate atom.

Algorithm A3: Grain-identification algorithm grouping areas of similarly oriented atoms into grain entities.

Data: *Position data for all atoms*

Result: *A certain number of grains*

```

1 foreach atom  $a$  do
2   if  $a$  has been assigned to any grain then
3     continue
4   end
5   new grain  $G$ 
6   empty atom list  $l_N$ 
7   empty atom list  $l_{NN}$ 
8   add  $a$  to  $l_N$  with  $a$  as parent atom
9   while number of entries of  $l_N > 0$  do
10    foreach atom  $a_n$  in  $l_N$  do
11      if  $a_n$  has been assigned to any grain then
12        continue
13      end
14      // local criterion
15      if  $a_n$  and its parent atom have not a very close orientation then
16        continue
17      end
18      // global criterion
19      if the orientation of  $a_n$  and the average orientation of  $G$  are not close then
20        continue
21      end
22      assign  $a_n$  to  $G$ 
23      add all nearest neighbors of  $a_n$  to  $l_{NN}$  with  $a_n$  as parent atom
24    end
25     $l_N = l_{NN}$ 
26     $l_{NN} =$  new empty list
27  end
28  if  $G$  does not comprise a sufficient amount of atoms then
29    dissociate all atoms of  $G$ 
30    delete  $G$ 
31  end
32 end

```

Appendix A.3. Orphan atom adoption

The atoms that were not successfully assigned to a grain by the previous algorithm are referred to as *orphan atoms*. The current algorithm is used to assign these atoms to a grain in a procedure deemed as atom adoption, which is based on the most frequent occurrences of the same grain. A threshold for the minimum number of occurrences of a grain was implemented to suppress a random pick behavior. The procedure is repeated for every atom until no further adoptions can occur in the dataset.

Algorithm A4: Algorithm assigning atoms to preexisting grains by taking into account the grain-membership of nearest neighbor atoms.

Data: *Position data for all atoms*

Result: *A certain number of grains*

```
1 foreach orphan atom  $a_{orph}$  do
2   count(all grains) = 0
3   if  $a_{orph}$  has been adopted by any grain then
4     | continue
5   end
6   foreach neighbor atom  $a_n$  to  $a_{orph}$  do
7     | if  $a_n$  is assigned to any grain then
8     | | count(grain( $a_n$ )) ++
9     | end
10  end
11  identify the grain  $g_{MF}$  with the highest count  $c_{MF}$ 
12  if  $c_{MF} \geq$  minimum number of grain occurrence then
13  | adopt  $a_n$  by  $g_{MF}$ 
13  | //  $a_n$  is now assigned to  $g_{MF}$ 
14  end
15 end
```

Appendix A.4. Grain tracking over time

Algorithm A5 finds a corresponding grain-entity from a previously analyzed data set. Both the center-of-mass (COM) and the orientation of the grains are utilized as criteria to match couples from the data sets.

Algorithm A5: Algorithm assigning a currently detected grain to a grain-entity from a previous timestep.

```

Input: a newly identified grain  $g$ 
Data:
  Volume  $V_G$  of the grain  $g$ 
  some factor  $a$ 
1 mapped grain  $g_{mapped}$  grain id  $id_G = NO\_GRAIN$ 
2  $d_{max} = a \left( \frac{V_G}{4/3\pi} \right)^{1/3}$ 
3  $d_{min} = d_{max}$ 
4 foreach Grain  $g_{prev}$  from the previous timestep do
5   if  $g_{prev}$  is already assigned to any grain then
6     | continue
7   end
8   // Center-of-mass distance-criterion
9    $d =$  distance between COM( $g$ ) and COM( $g_{prev}$ )
10  if  $d > d_{max}$  then
11    | continue
12  end
13  // Misorientation-criterion
14   $\Delta\varphi =$  misorientation between the average orientations of  $g$  and  $g_{prev}$ 
15  if  $\Delta\varphi > \Delta\varphi_{max}$  then
16    | continue
17  end
18  // All criteria fulfilled
19  if  $d \leq d_{min}$  then
20    |  $d_{min} = d$ 
21    |  $g_{mapped} = g_{prev}$ 
22    |  $id_G = id(g_{prev})$ 
23  end
24 end
25 if  $id_G \neq NO\_GRAIN$  then
26   | // do not allow a double assignment
27   | set  $g_{mapped}$  as assigned
28   | return  $id_G$ 
29 end
30 return a new id

```

Appendix A.5. Rotation quaternions and unique orientations

During the determination of the per-atom orientation, owing to the symmetry of the cubic lattice different but equivalent orientation quaternions may be calculated. For this reason, it is necessary to reduce the orientation to a unique one. This done by algorithm A6 by the utilization of Eqs. (A.1)-(A.24):

Algorithm A6: Algorithm to obtain the unique cubical orientation quaternion q_{uo} to a quaternion q .

Input: An orientation quaternion q

- 1 Cosine Angle $C_{max} = 0$
- 2 The unique quaternion to identify q_u
- 3 **foreach** 24 cubically equivalent quaternions q_i to q **do**
- 4 **if** $|q_i[0]| > C_{max}$ **then**
- 5 $C_{max} = |q_i[0]|$
- 6 $q_u = q_i$
- 7 **end**
- 8 **end**
- 9 **if** $q_u[0] < 0$ **then**
- 10 $q_u = -q_u$
- 11 **end**
- 12 **return** q_u

List of the 24 cubically-equivalent orientation quaternions:

$$q_1^T = [a_0; a_1, a_2, a_3] \quad (\text{A.1})$$

$$q_2^T = [-a_1; a_0, a_3, -a_2] \quad (\text{A.2})$$

$$q_3^T = [-a_2; -a_3, a_0, a_1] \quad (\text{A.3})$$

$$q_4^T = [-a_3; a_2, -a_1, a_0] \quad (\text{A.4})$$

$$q_5^T = 0.5[a_0 - a_1 - a_2 - a_3; a_0 + a_1 + a_2 - a_3, a_0 - a_1 + a_2 + a_3, a_0 + a_1 - a_2 + a_3] \quad (\text{A.5})$$

$$q_6^T = 0.5[a_0 + a_1 + a_2 + a_3; -a_0 + a_1 - a_2 + a_3, -a_0 + a_1 + a_2 - a_3, -a_0 - a_1 + a_2 + a_3] \quad (\text{A.6})$$

$$q_7^T = 0.5[a_0 - a_1 + a_2 - a_3; a_0 + a_1 + a_2 + a_3, -a_0 - a_1 + a_2 + a_3, a_0 - a_1 - a_2 + a_3] \quad (\text{A.7})$$

$$q_8^T = 0.5[a_0 + a_1 - a_2 + a_3; -a_0 + a_1 - a_2 - a_3, a_0 + a_1 + a_2 - a_3, -a_0 + a_1 + a_2 + a_3] \quad (\text{A.8})$$

$$q_9^T = 0.5[a_0 + a_1 - a_2 - a_3; -a_0 + a_1 + a_2 - a_3, a_0 - a_1 + a_2 - a_3, a_0 + a_1 + a_2 + a_3] \quad (\text{A.9})$$

$$q_{10}^T = 0.5[a_0 - a_1 + a_2 + a_3; a_0 + a_1 - a_2 + a_3, -a_0 + a_1 + a_2 + a_3, -a_0 - a_1 - a_2 + a_3] \quad (\text{A.10})$$

$$q_{11}^T = 0.5[a_0 + a_1 + a_2 - a_3; -a_0 + a_1 + a_2 + a_3, -a_0 - a_1 + a_2 - a_3, a_0 - a_1 + a_2 + a_3] \quad (\text{A.11})$$

$$q_{12}^T = 0.5[a_0 - a_1 - a_2 + a_3; a_0 + a_1 - a_2 - a_3, a_0 + a_1 + a_2 + a_3, -a_0 + a_1 - a_2 + a_3] \quad (\text{A.12})$$

$$q_{13}^T = \frac{1}{\sqrt{2}}[a_0 - a_1; a_0 + a_1, a_2 + a_3, -a_2 + a_3] \quad (\text{A.13})$$

$$q_{14}^T = \frac{1}{\sqrt{2}}[a_0 - a_2; a_1 - a_3, a_0 + a_2, a_1 + a_3] \quad (\text{A.14})$$

$$q_{15}^T = \frac{1}{\sqrt{2}}[a_0 - a_3; a_1 + a_2, -a_1 + a_2, a_0 + a_3] \quad (\text{A.15})$$

$$q_{16}^T = \frac{1}{\sqrt{2}}[-a_1 - a_2; a_0 - a_3, a_0 + a_3, a_1 - a_2] \quad (\text{A.16})$$

$$q_{17}^T = \frac{1}{\sqrt{2}}[-a_2 - a_3; a_2 - a_3, a_0 - a_1, a_0 + a_1] \quad (\text{A.17})$$

$$q_{18}^T = \frac{1}{\sqrt{2}}[-a_1 - a_3; a_0 + a_2, -a_1 + a_3, a_0 - a_2] \quad (\text{A.18})$$

$$q_{19}^T = \frac{1}{\sqrt{2}}[a_0 + a_1; -a_0 + a_1, a_2 - a_3, a_2 + a_3] \quad (\text{A.19})$$

$$q_{20}^T = \frac{1}{\sqrt{2}}[a_0 + a_2; a_1 + a_3, -a_0 + a_2, -a_1 + a_3] \quad (\text{A.20})$$

$$q_{21}^T = \frac{1}{\sqrt{2}}[a_0 + a_3; a_1 - a_2, a_1 + a_2, -a_0 + a_3] \quad (\text{A.21})$$

$$q_{22}^T = \frac{1}{\sqrt{2}}[a_1 - a_2; -a_0 - a_3, a_0 - a_3, a_1 + a_2] \quad (\text{A.22})$$

$$q_{23}^T = \frac{1}{\sqrt{2}}[a_2 - a_3; a_2 + a_3, -a_0 - a_1, a_0 - a_1] \quad (\text{A.23})$$

$$q_{24}^T = \frac{1}{\sqrt{2}}[a_1 - a_3; -a_0 + a_2, -a_1 - a_3, a_0 + a_2] \quad (\text{A.24})$$